Overtone Mobility Spectrometry: Part 1. Experimental Observations

Ruwan T. Kurulugama, Fabiane M. Nachtigall, Sunyoung Lee, Stephen J. Valentine, and David E. Clemmer
Department of Chemistry, Indiana University, Bloomington, Indiana, USA

A new method that allows a linear drift tube to be operated as a continuous ion mobility filter is described. Unlike conventional ion mobility instruments that use an electrostatic gate to introduce a packet of ions into a drift region, the present approach uses multiple segmented drift regions with modulated drift fields to produce conditions that allow only ions with appropriate mobilities to pass through the instrument. In this way, the instrument acts as a mobility filter for continuous ion sources. By changing the frequency of the applied drift fields it is possible to tune this instrument to transmit ions having different mobilities. A scan over a wide range of drift field frequencies for a single ion species shows a peak corresponding to the expected resonance time of the ions in one drift region segment and a series of peaks at higher frequencies that are overtones of the resonant frequency. The measured resolving power increases for higher overtones, making it possible to resolve structures that were unresolved in the region of the fundamental frequency. We demonstrate the approach by examining oligosaccharide isomers, raffinose and melezitose as well as a mixture of peptides obtained from enzymatic digestion of myoglobin. (J Am Soc Mass Spectrom 2009, 20, 729–737) © 2009 Published by Elsevier Inc. on behalf of American Society for Mass Spectrometry

Separation of a mixture of ions by ion mobility spectrometry (IMS) in linear drift tubes is initiated by gating short packets of ions into the front of a drift region containing a static buffer gas. Different species then migrate through the drift region under the influence of an applied field according to their mobilities in the buffer gas, such that ions with high mobilities reach the detector before those with low mobilities [1–6]. This approach has attracted considerable attention as a means of analyzing complex mixtures [7–16]. Additionally, measured mobilities can be converted to experimental cross sections and comparison of these values with cross sections for model geometries that are calculated can be used to characterize ion structures [17–28].

In this report we introduce a new approach for isolating ions having specific mobilities (or collision cross sections). Ions from a continuous source enter a drift tube with segmented drift regions. The drift fields are modulated at a frequency that allows only those ions having mobilities that are resonant with the experimental conditions to be transmitted through all drift regions. In this way, this device filters away all ions except those with mobilities over the selected narrow range. An unanticipated feature of this approach is the observation that ions can be passed at overtone frequencies; moreover, the resolving power in higher overtone regions is greater than that observed in the fundamental frequency range. Because of the ability to select ions in different frequency regions, including those that are associated with higher overtones, we refer to the approach as *overtone mobility spectrometry* (OMS).

To demonstrate this approach we have examined two types of systems. First, we show that different ions from a simple ESI source are favored at different frequencies. This is done for two trisaccharides (raffinose and melezitose, which are structural isomers). We find that it is relatively straightforward to favor one or the other from a mixture of the two. We then examine the utility of OMS as a means of simplifying a more complicated mixture of tryptic peptides (from a digest of myoglobin).

The separation and selection of ions according to their mobilities currently constitute an area of significant research activity and numerous other techniques are being developed, including differential mobility analysis, in which ions migrate through a flowing gas under the influence of a field [29–31], and field asymmetric (FA) IMS, which separates ions based on differences between high- and low-field mobilities [32–38]. Such approaches are finding applications as a means of characterizing a range of analytes—from chemical warfare agents to determining particle sizes—and also have

Address reprint requests to Dr. David E. Clemmer, Indiana University, Department of Chemistry, 800 E. Kirkwood Ave., Bloomington, IN 47405. E-mail: clemmer@indiana.edu

1044-0305/09/$32.00
doi:10.1016/j.jasms.2008.11.022

Published online December 6, 2008
Received August 28, 2008
Revised November 21, 2008
Accepted November 25, 2008

utility as a means of simplifying the analysis of complex mixtures through the removal of chemical noise (or other components of the mixture that differ in mobility) [1, 10, 31, 39–45]. The OMS approach described here should also be useful for these types of applications. One advantage of the approach is that it is rooted in a fundamental property of the ion (its mobility), making it possible to tune the filter for selection of desired species.

Experimental

General

Detailed descriptions of IMS [1, 2, 4, 6, 39, 46, 47] and IMS-MS [2, 3, 48–54] instrumentation as well as theoretical considerations are provided elsewhere [5, 6, 22–24, 55, 56]. Additionally, instrumentation components including the ion source, ion focusing elements, vacuum system, mass spectrometer, detection scheme, and recent instrumentation modifications leading to the current instrument are discussed elsewhere [57–60]. Here, a description of the experimental apparatus focuses on the multisegmented drift tube. Figure 1a shows a schematic diagram of the drift tube mass spectrometer used in these studies. Ions are produced using a home-built electrospray ionization (ESI) source and are continuously focused through an ion funnel (F1) interface into a linear drift region. The drift region is 181 cm long and can be configured to operate using a uniform field (as described previously) [59, 60] or alternating fields applied to segmented drift regions (as described in more detail in the following text). Ions that exit the drift tube are focused into the source region of a reflectron time-of-flight (TOF) mass spectrometer for mass analysis.

Sample Preparation

Raffinose (98% purity), melezitose (99% purity), and horse myoglobin (≥90% purity) were purchased from Sigma Chemical (St. Louis, MO, USA) and used without further purification. Raffinose and melezitose (0.25 $mg \cdot mL^{-1}$) were prepared in water:acetonitrile (50:50% by volume) and 2 mM NaCl. Tryptic peptide mixtures were obtained as follows. Myoglobin was initially dissolved in 6 M urea buffer and the sample was diluted to 2 M urea using 0.2 M Tris buffer (pH = 8.0, 10 mM $CaCl_2$) before trypsin digestion. Tryptic peptides were generated by adding TPCK-treated trypsin (2% enzyme by mass to that of the protein) and incubating the solution at 37 °C for 24 h. Finally, the mixture of peptides was desalted using Oasis hydrophilic-lipophilic balanced (HLB) cartridges (Waters Inc., Milford, MA, USA) and dried on a centrifugal concentrator. Dried peptides were resuspended in water:acetonitrile: acetic acid solution (49:49:2% by volume).

Segmented Drift Tube and Ion Funnel Assembly

Figure 1b shows a schematic diagram of the segmented drift tube. The midsection of the drift tube has been divided into 22 segments. Of these, 21 segments are identical. Each segment is composed of five concentric stainless steel rings (14.0 cm o.d.; 7.0 cm i.d.). The first two contain grids (90% transmittance, Ni mesh grid, Buckbee-Mears, St. Paul, MN, USA) and are separated by a 0.18-cm-thick Teflon isolator (14.0 cm o.d.; 8.3 cm i.d.). The remaining three lenses are separated by 1.27-cm-thick Delrin spacers (14.0 cm o.d.; 8.3 cm i.d.). The rings and spacers are stacked together, sealed with O-rings, and compressed using eight nylon threaded rods; multiple segments are joined to create the mobility filter region. The length of each segment (from the front grid of one segment to the front grid of an adjacent segment) is 5.84 cm and so the total length of the 22-section separation region is 128.5 cm.

One segment near the center of the drift tube is replaced by an ion funnel assembly that is similar to published designs [53, 60]. This ion funnel is made of 22 stainless steel electrodes (0.075 cm thick; 12.7 cm o.d.), with aperture diameters that decrease linearly from 7.00 to 0.56 cm; the funnel lenses are separated by 0.18-cm-thick Teflon spacers. The funnel is designed such that its total length (5.74 cm) is similar to that of the individual drift tube segments. The funnel is operated using radio-frequency (RF) fields of 50–70 $V_{p\text{-}p}$ at 450 kHz and 10 $V \cdot cm^{-1}$ DC field. With the exception of the RF component used to improve ion transmission through the drift tube device, the funnel is used here simply as an additional drift segment. Evidence that the ion transit times through the funnel region are similar to the other drift regions is obtained from two observations. First, the placement of an ion funnel in the OMS device at various positions does not significantly change peak widths, peak positions, or peak intensities, even when using two ion funnels. The second observation is that accurate collision cross sections can be obtained from OMS measurements that use in-line ion funnels. The assembly of lenses and spacers forms a cavity that can be filled with a buffer gas. Helium was used as the buffer gas and typically the pressure was 2.25 Torr, as determined by a capacitance manometer. The buffer gas temperature was about 298 K.

Modulation of Drift Fields in the Segmented Drift Tube

A uniform, 10 $V \cdot cm^{-1}$ DC field is created across each segment using a combination of applied voltages and appropriate resistors in series (57 kΩ, 1% tolerance). In the present system, fields are applied to pairs of segments (i.e., voltage is applied at the front of each segment pair) to create a sawtooth (Figures 1a and 1b) voltage gradient down the axis of the drift tube. A second sawtooth is offset from the first by one segment and is turned on while the first sawtooth field is turned

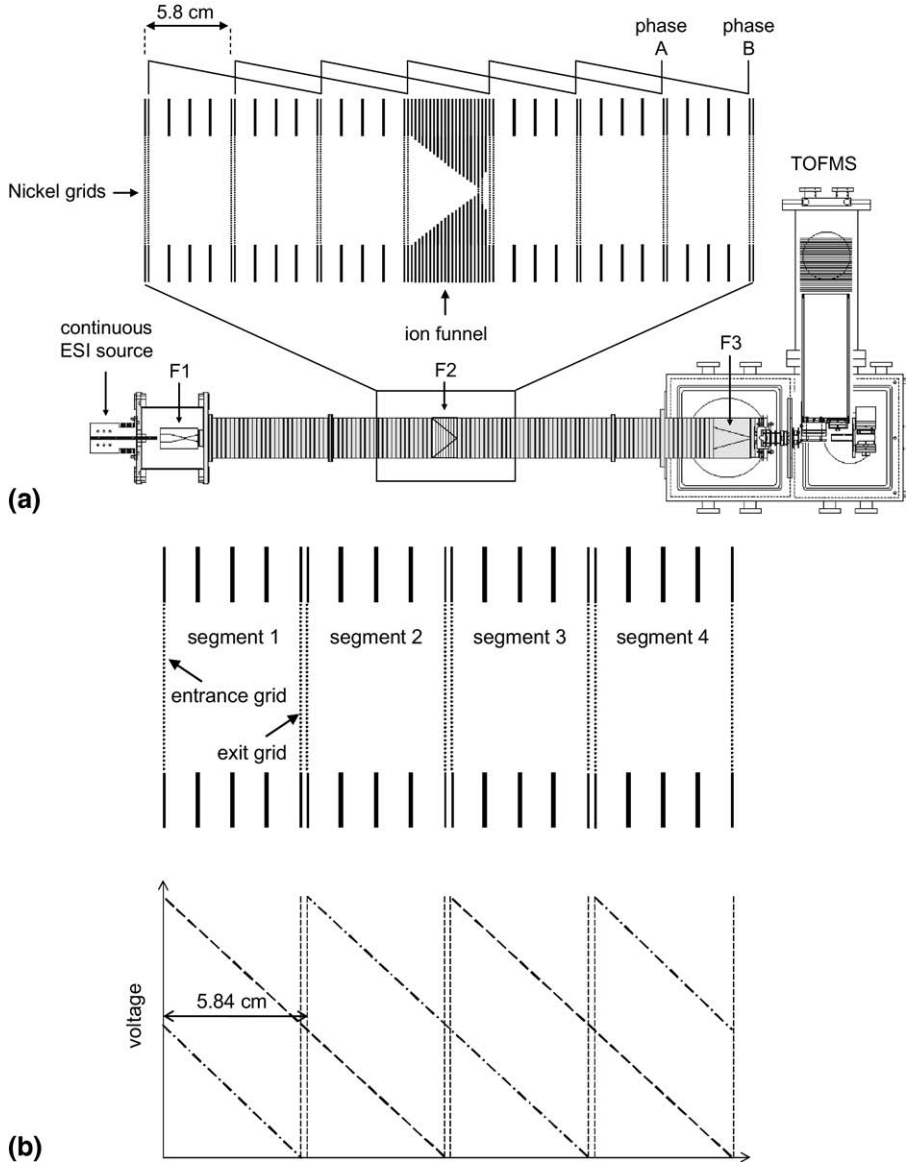

Figure 1. Schematic diagram of the drift tube mass spectrometer used in these studies (**a**). The instrument incorporates an ESI ion source, three ion funnels (labeled F1 to F3), a segmented drift region, and a time-of-flight mass spectrometer. Upon application of a linear field (and gating ions at F1 as described previously) it is possible to record traditional ion mobility/mass spectra. However, the middle region of the instrument is divided into segments, as shown in detail in the inset of the figure. This region consists of 22 sections that are separated by Ni grids. The drift field of each section is controlled by a two-phase circuit. When the segmented region is operated at a specific field application frequency, it is possible to continuously transmit ions of a specific mobility. See text for details. (**b**) Schematic diagram showing the details of the segmented drift tube (top) and the overlap of the voltage gradients on the drift tube for the two sawtooth waves (bottom). The dashed line corresponds to the first sawtooth wave (phase A) and the dashed-dotted line corresponds to the second sawtooth (phase B). Here the application of the two phases is modulated at different frequencies to allow for the transmission of different ions through the drift tube. For this drift tube setup, the drift field is kept at 10 $V \cdot cm^{-1}$. At this drift field, the space between two sections (between two adjacent grids) consists of 114.4 V, giving a field of -477 $V \cdot cm^{-1}$. The region containing the negative field essentially acts as an ion elimination region.

off. These fields are alternated at a frequency that is referred to as the drift field application frequency.

As mentioned earlier, the separation of ions in this instrument occurs based on the mobilities of the ions analyzed. However, in contrast to a conventional drift tube experiment, the separation is recorded in the frequency domain. The frequency here corresponds to the speed at which the two drift field settings or phases (the phase of the OMS system refers to the number of distinct field settings) are modulated. For example, for a

two-phase system, at 2000 Hz field application frequency, one phase is turned on for 500 μs, whereas the other is turned off for the same amount of time and the two phases are alternately turned on and off to move the ions across the drift tube. Since the ion transmission is a function of frequency, a plot of frequency versus the signal intensity for a given ion constitutes its OMS spectrum.

For a given ion, the positions of the peaks appearing at higher frequencies are related to multiples of the fundamental frequency. The appearance of these overtone peaks demonstrates that ions can be stable inside the drift tube not only at the fundamental frequency but also at other frequencies that are multiples (termed harmonics) of the fundamental frequency. For a two-phase system, overtone peaks appear at $3f_f$, $5f_f$, $7f_f$, and so forth of the fundamental frequency. A thorough explanation for the appearance of the overtone peaks, their positions, and the dependence on the number of phases used for the experiment will be given in an accompanying article describing theoretical considerations of the resolving power of OMS.

Results and Discussion

Example Mass Spectra Obtained upon ESI of Raffinose into Segmented Drift Tube

Figure 2 shows mass spectra that have been recorded upon direct electrospray of a solution containing the three-residue oligosaccharide raffinose. By applying a constant electric field across all segments of the OMS, a mass spectrum (Figure 2a) is obtained containing a number of prominent peaks. The spectrum is dominated by a peak mass-to-charge (*m/z*) 527. Other smaller peaks at 532.5 and 1031 are also observed. By examining the isotopic patterns for these ions, it is possible to determine their charge state. Isotopes observed for the feature at *m/z* 527 are spaced by 1 *m/z*, indicating this species is singly charged. Based on the charge state and the *m/z* value, we assign this ion as the $[M + Na]^+$ monomer ion of raffinose. A spacing of 0.5 Th within the isotopic envelope for the feature at *m/z* 532.5 indicates that it is a doubly charged ion. Currently this ion has not been assigned. The peak observed at *m/z* 1031 can nominally be assigned to the $[2M + Na]^+$ dimer. However, the congested isotope pattern suggests that higher-order multimers (e.g., $[4M + 2Na]^{2+}$ and $[6M + 3Na]^{3+}$) are also present. The discussion presented in the following text addresses the assignment of these species.

Upon application of modulated field settings to the OMS drift tube as described earlier, we observe very different ion distributions. For example, application of the drift field settings at a rate of 2050 Hz yields a mass spectrum in which the 532.5 peak is eliminated. These conditions seem to favor a small population of ions in the approximately 790–805 *m/z* range. At nearly 1400 or 2550 Hz the 1031 or 532.5 peaks are favored. Such a strong frequency dependence of the observed ion distribution was initially very surprising. The result suggests the possibility of obtaining distributions as a function of frequency for each ion by monitoring the intensity of each mass spectral feature as a function of applied frequency.

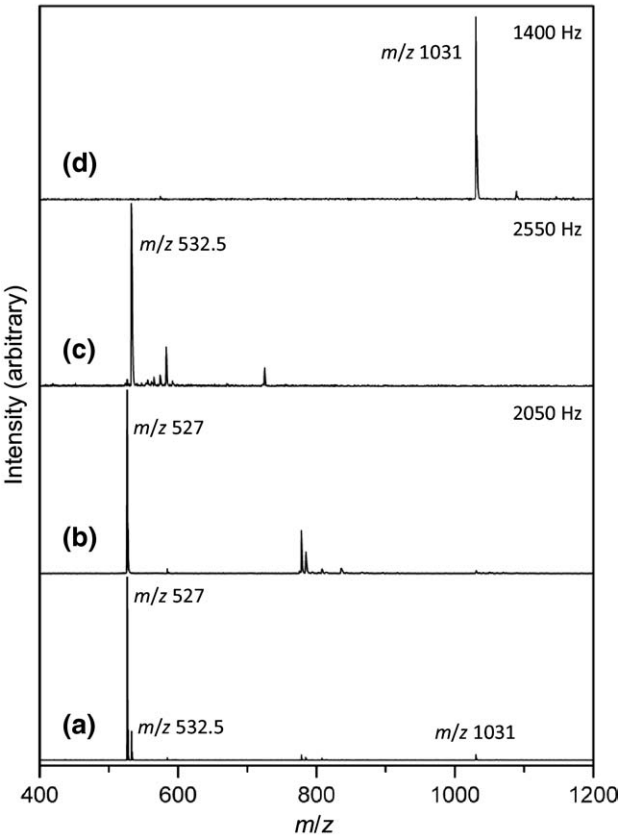

Figure 2. Mass spectra obtained upon ESI of raffinose. The bottom spectrum (**a**) shows the total mass spectrum obtained when the instrument is operated as a conventional drift tube. The top three mass spectra are obtained by operating the OMS instrument at different frequencies. When the OMS instrument is operated at 1400 Hz (**d**), the dominant peak in the mass spectrum is *m/z* 1031 ion (this corresponds to $[2M + Na]^+$; however, at different field application frequencies, $[4M + 2Na]^{2+}$ and $[6M + 3Na]^{3+}$ ions also can be observed that correspond to the same *m/z* value; see text for more detail). When the operating frequency is 2050 Hz (**b**), singly charged raffinose monomer becomes the dominating ion, whereas at 2550 Hz (**c**) the instrument selectively transmits the *m/z* 532.5 ion.

Examples of the Frequency Dependence of Several Different Ions

Figure 3 shows several examples of OMS spectra obtained for specific ions upon scanning the drift-field application frequency. In this case the frequency has been varied from close to 0 to about 16,000 Hz. The plot shows the ion intensities that are recorded for the 527, 532.5, and 1031 ions mentioned earlier. Over this range of frequencies, the OMS spectrum for $[M + Na]^+$ (*m/z* 527) is dominated by a large peak at 2050 Hz. A much

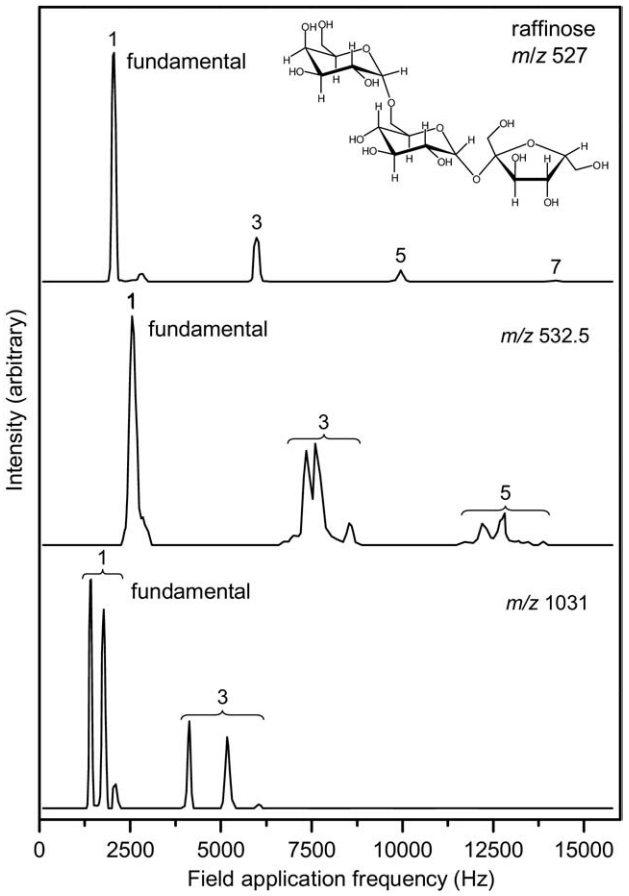

Figure 3. Measured ion intensity (arbitrary units) as a function of field application frequency over a range of close to 0 to about 16,000 Hz obtained upon ESI of a 0.25 mg/mL solution of raffinose. The top spectrum corresponds to the sodiated monomer of raffinose. The peak labeled *fundamental* occurs at a frequency that corresponds to transmission of ions through the distance of a single section of the drift region (in this case one of the 5.84-cm segments shown in Figure 1). The complicated pattern of peaks observed at higher frequencies corresponds to transmission of ions at specific overtones (and the numerical labels indicate the harmonic factor of the overtone; see text for more detail). This sample also showed peaks for *m/z* 1031 ion (bottom spectrum) and an unassigned ion with a *m/z* value of 532.5 (middle spectrum).

smaller peak is observed at 2750 Hz. Smaller peaks that decrease in intensity with increasing frequency are observed at 5977, 9952, and 14,194 Hz.

The doubly charged ion having *m/z* 532.5 (unassigned ion from the raffinose sample) shows a more complicated pattern of peaks (see Figure 3). The most prominent peak is centered at 2571 Hz and is slightly broader than the peaks observed for the $[M + Na]^+$ ion. Additionally, this peak shows a small reproducible feature at higher frequencies (the shoulder at ~2846 Hz). As the frequency is increased, two additional sets of smaller peaks (at 7383, 7656, and 8555 Hz, as well as 12,247, 12,734, and 13,894 Hz, respectively) are observed. Again, in general, peak intensities decrease with increasing frequency.

The OMS distribution for the *m/z* 1031 ion shows three sharp peaks at 1398, 1760, and 2068 Hz (Figure 4). Because the isotopic envelope suggested the presence of multiple isobaric species, we have examined the isotopic envelopes of the frequency-resolved ions. This shows that isotopic peaks are spaced by 1.0, 0.5, and 0.33 Th for the features observed at 1398, 1760, and 2068 Hz, respectively. With this charge state information, we assign these species to the singly charged dimer $[2M + Na]^+$, the doubly charged tetramer $[4M + 2Na]^{2+}$, and the triply charged hexamer $[6M + 3Na]^{3+}$ ions, respectively. Additional peaks in the OMS distribution are observed at higher frequencies, including: 4135, 5182, and 6062 Hz. The intensities of these higher-frequency peaks are smaller than those of the lower-frequency peaks. The isotopic spacing of these peaks allows them

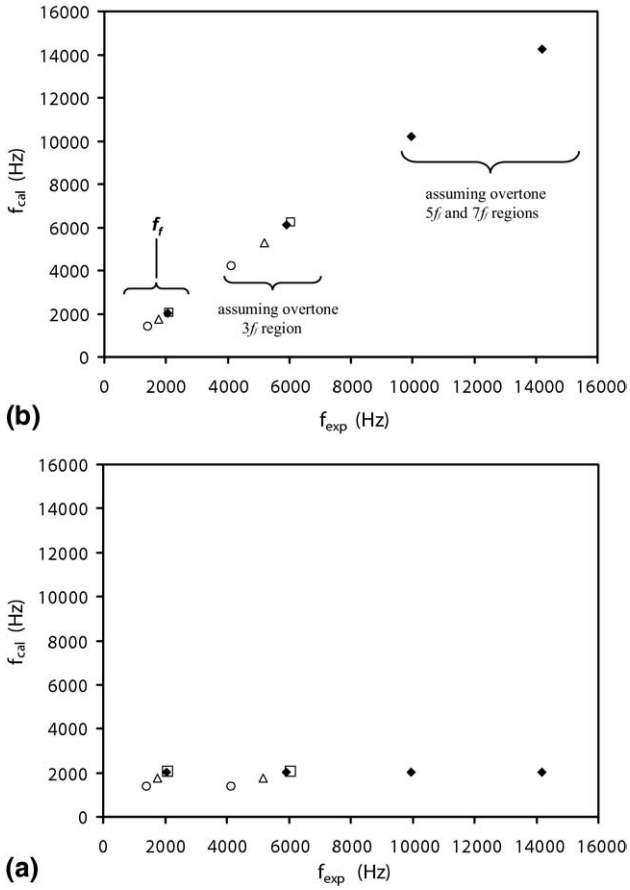

Figure 4. Plot of calculated field application frequency with respect to experimental field application frequency for raffinose $[M + Na]^+$ (solid diamond), $[2M + Na]^+$ (open circle), $[4M + 2Na]^{2+}$ (open triangle), and $[6M + 3Na]^{3+}$ (open square). The calculated frequency is obtained by calculating the time it takes for these ions to travel the distance of one segment (5.84 cm) and taking the inverse of that value (based on the drift time values obtained for these ions when the instrument is operated as a conventional drift tube). (**a**) The plot obtained when the calculated frequency is not corrected to reflect the frequencies obtained at higher overtone levels. However, when the calculated values obtained for higher overtone levels are multiplied by the harmonic integer value (e.g., 3, 5, and 7), the resultant plot shows a trend line with a correlation coefficient of 0.9996 and a slope of 1.0063, showing a better agreement with the calculated and experimental frequency values (**b**). These results are obtained for a two-phase system.

to be assigned as $[2M + Na]^+$ (4135 Hz), $[4M + 2Na]^{2+}$ (5182 Hz), and $[6M + 3Na]^{3+}$ (6062 Hz). This spectrum for these ions is very interesting and can be used to develop a working understanding of this instrumentation. Specifically, these data show that multiply charged multimers of the same nominal *m/z* value are transmitted at different frequencies. Moreover, the peaks appear as two groups. Each of the peaks in the higher-frequency groups appears at a frequency that is about a factor 3 higher than the lower-frequency transmission value. That is, $4135/1398 \approx 2.96$ and $6062/2068 \approx 2.93$. This suggests that each ion is being transmitted at a fundamental frequency as well as at an overtone frequency. The observation of overtone peaks resulted in naming this approach as *overtone mobility spectrometry* (OMS). Finally, we find it very interesting that, although the positions of peaks change by multiples of the fundamental frequency, the peak widths do not. This leads to the observation that the resolving power of OMS increases in higher overtone regions of the spectrum.

Understanding the Origin of Higher Frequency Peaks

It is important to understand the origin of the transmission frequencies. For example, using IMS measurements for the $[M + Na]^+$ monomer of raffinose, a drift time (t_D) of 15.2 ms is obtained. This is the time required for the ion to traverse the entire 181-cm linear IMS drift tube. Using this information, it is possible to calculate the ion displacement during the time required for application of a single field setting at the frequency giving rise to the most dominant peak (Figure 4) in the OMS spectrum. Here, a frequency of 2050 Hz corresponds to a field application time of nearly 488 μs. Using the measured drift velocity of the ion (1.19×10^4 $cm \cdot s^{-1}$), the distance traveled during a single field setting would be 5.81 cm. This is almost identical to the value of one drift segment (in this case 5.84 cm).

Using the measured t_D values for species observed in the raffinose sample, it is possible to calculate frequencies for which the peaks are observed in the OMS distribution. Consider the raffinose multimer ions in the OMS spectrum where three distinct features are observed at lower-frequency settings (<2500 Hz). The IMS drift distribution profile for this ion also shows three baseline-resolved peaks having intensities that increase with increasing drift time. In contrast, the peaks in the OMS spectrum exhibit a decreasing intensity pattern for these peaks. Using the method described earlier, calculated OMS frequencies of 2070, 1760, and 1401 Hz are obtained for peaks with t_D values of 15.0, 17.6, and 22.1 ms, respectively. These values are close to the experimental values of 2068, 1760, and 1398 Hz.

Figure 4 shows a plot of calculated frequencies versus experimentally determined frequencies for a number of the ions observed from the raffinose sample. We provide two examples of this plot. The first (Figure 4a) assumes no overtones. In this case only the fundamental experimental transmission frequencies correlate directly with values calculated from IMS measurements. If the higher-frequency (>3000 Hz) features in the OMS distributions are multiplied by the appropriate integer value (3, 5, or 7), we obtain Figure 4b. The correlation coefficient for the plot shown in Figure 4 is 0.9996 and the slope is 1.0063, indicating that in all cases, multiples of the calculated frequency for the same ion give rise to the observed peaks at higher frequencies in the OMS spectra. Hereafter, we refer to the frequency corresponding to an ion traversing one drift tube segment as the *fundamental frequency* (f_f) and the higher-frequency settings as *overtones*. For these data, peaks associated with overtone frequencies of $3f_f$, $5f_f$, and $7f_f$ are observed (Figure 3).

Observation of Enhanced Resolving Power for Higher Overtone Regions

The resolving power of OMS is defined by $(f/\Delta f)$, where f corresponds to the frequency at which maximum ion intensity is transmitted, and Δf is taken as the width of the OMS peak at half maximum. In general, the OMS resolving power is observed to increase with increasing overtone number. Consider the peaks for the $[2M + Na]^+$, $[4M + 2Na]^{2+}$, and $[6M + 3Na]^{3+}$ ions having *m/z* 1031 shown in Figure 3. The OMS resolving power values obtained for the three f_f peaks are 15.3, 15.1, and 15.4 for the dimer, tetramer, and hexamer, respectively. The resolving power values obtained for the $3f_f$ overtone peaks for the same ions (in the same order) are 40.3, 35.2, and 41.6. This type of increase in resolving power with overtone number is typical. A separate example is the doubly charged ion (*m/z* 532.5). The f_f setting exhibits a single, relatively broad peak and yields a measured resolving power of 10.8. The resolving power for the $3f_f$ overtone peaks give values of 27.6, 28.6, and 39.6 for peaks centered at 7383, 7656, and 8555 Hz, respectively. The resolving power for the peaks at 12,247 and 12,734 Hz is 44.0 and 62.8, respectively. There is a small signal at 13,874 Hz, the expected position for the $5f_f$ overtone of the third peak, which suggests even higher resolving power. These results demonstrate the utility of operating the instrument at higher overtone frequencies to isolate ions of specific mobilities.

An Example Separation of the Structural Isomers of Raffinose and Melezitose

As another example, we illustrate the utility of enhanced resolving power at higher overtones by examining the separation of structural isomers. Figure 5 shows OMS distribution plots for raffinose (top), melezitose (middle), and a mixture at 3:1 raffinose:melezitose (bottom). From high-resolution IMS measure-

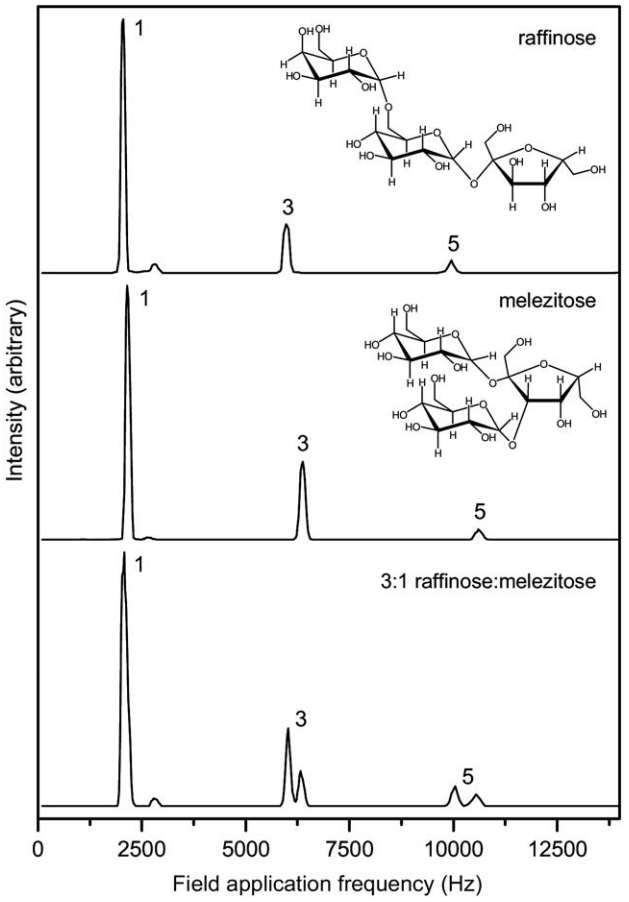

Figure 5. A comparison of measured ion intensities as a function of field application frequency over a range of close to 0 to about 14,000 Hz for raffinose, melezitose, and a mixture of raffinose and melezitose at 3:1 ratio. The data are collected using a two-phase wave-driving circuitry. Here, the peaks for the f_f, $3f_f$, and $5f_f$ frequencies are shown for all three spectra. The two isobaric trisaccharides are not resolved at the f_f (bottom spectrum). However, at the $3f_f$ and $5f_f$ overtone frequencies these two ions are partially and baseline resolved, respectively. The structures of the native molecules are also given on each spectrum.

ments, we know that raffinose has a slightly lower mobility than that of melezitose, allowing a mixture of these two ions to be separated in a conventional drift tube with sufficient resolving power [61]. The frequency spectrum obtained for the trisaccharide mixture also shows that. Although, the two isomers are not resolved in the fundamental region of the spectrum, they are partially and fully resolved at the $3f_f$ and $5f_f$ overtone frequency regions, respectively. Thus, even at this very early stage of development, this becomes an interesting approach. In this case, a very simple means of selecting isomers would be useful for tandem MS types of analyses.

Separation of Peptides from a Tryptic Digest of Myoglobin

As a final example, we consider a more complex mixture of tryptic peptides generated upon enzymatic digestion with trypsin. Several results are shown in Figure 6. When the drift tube is configured as a traditional IMS instrument, we observe the complicated pattern of peaks associated with forming the $[M + H]^+$, $[M + 2H]^{2+}$, and $[M + 3H]^{3+}$ peptides upon electrospray. For reference, we have indicated the positions and assignments of several large peaks, $[ALELFR + 2H]^{2+}$ at m/z = 374.7, $[HGTVVLTALGGILK + 3H]^{3+}$ at m/z = 460.2, and $[YLEFISDAIIHVLHSK + 3H]^{3+}$ at m/z = 628.9. When the multiple drift region configuration is used, it is straightforward to find conditions where only a narrow band of mobility-selected ions is transmitted. For example, mass spectra recorded at 6000, 7000, or 8000 Hz are largely dominated by single peaks corresponding to $[YLEFISDAIIHVLHSK + 3H]^{3+}$, $[HGTVVLTALGGILK + 3H]^{3+}$, or $[ALELFR + 2H]^{2+}$, respectively. These data illustrate the selectivity of the approach. This could have utility in applications that seek to resolve specific conformations or isomers for subsequent analysis—for example, an OMS selection followed by collision-induced dissociation (CID) and MS analysis.

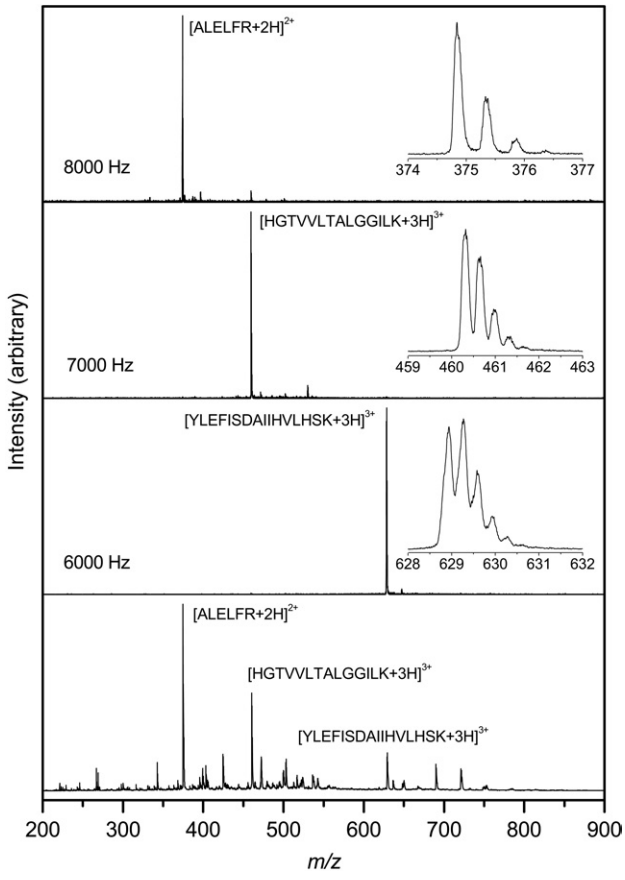

Figure 6. Mass spectra obtained upon ESI of a mixture of tryptic peptides of myoglobin at application frequencies of 6000, 7000, and 8000 Hz as well as the total mass spectrum (bottom). At different field application frequencies different ions are stable inside the drift tube. Therefore, this instrument acts as a mobility filter for a continuous ion source. The isotopic peak distribution for each ion is also provided on the spectrum that was used to identify the charge state of the ion.

To further illustrate the application of this technique for complex sample analysis, we have analyzed a tryptic digest of three proteins: myoglobin (horse), hemoglobin (human), and cytochrome c (human) and spiked with substance P peptide. A two-dimensional frequency (m/z) distribution for this tryptic digest is shown in Supplementary Figure S1, which can be found in the electronic version of this article. Here, the peak capacity for the fundamental peak range is calculated to be about 7, whereas for the $5f_f$ overtone frequency level the peak capacity is close to 27 and for the $9f_f$ overtone frequency level the peak capacity is about 36. Therefore, it is important to note the advantage of this technique for complex sample analysis, especially when using a higher overtone range.

Ion Signal

One final issue that we have not addressed so far is associated with ion signal. Ultimately the resolution that is obtained with this technique comes at the cost of a decreased signal. Some loss is incurred because this method acts as a filter. Thus, at a given transmission frequency setting, many ions will be lost. This is analogous to losses associated with selection of ions in a quadrupole mass filter. Another source of ion loss in the present work arises from the use of grids between each drift region. Although we have used 90% transmittance grids for this proof of concept, we anticipate that higher transmission grids (to a limit of gridless) designs will further improve this system. We are currently working on these designs.

Conclusion

A new ion-mobility separation approach that uses a segmented drift tube has been presented. In this approach, linear voltage gradients are applied to pairs of drift region segments in a fashion that creates a sawtooth pattern down the axis of the drift tube. The position of the sawtooth field is shifted between two sets of drift tubes such that only ions having mobilities that are in resonance with the switching frequency are passed through the instrument. In this way the device acts as a mobility filter. The approach has been demonstrated using several ions that are formed upon ESI of the oligosaccharide isomers raffinose and melezitose. A surprising finding is that it is possible to transmit ions at overtone frequencies and the peaks that are observed at higher overtones are sharp. This result is striking and raises the possibility of developing relatively simple, high-resolving-power mobility filters. The ability to select ions from continuous sources based on their mobilities is likely to find applications when combined with other scanning mass spectrometric devices, such as quadrupoles and trapping instruments. Further work involving the development of these instruments is ongoing.

Acknowledgments

The development of new instrumentation is supported in part by grants from the National Institutes of Health (AG-024547-01 and P41-RR018942) and the METACyte initiative, funded by a grant from the Lilly Endowment. The authors are grateful for numerous stimulating discussions with their colleagues, Liang-shi Li, Caroline C. Jarrold, and Gary M. Hieftje about overtones and instrumentation in general. We also thank John Poehlman and Andrew Alexander for technical support.

References

1. For a review of IMS techniques see for example (and references therein): St. Louis, R. H.; Hill, H. H., Jr. Ion Mobility Spectrometry in Analytical Chemistry. *Crit. Rev. Anal. Chem.* **1990,** *21,* 321–355.
2. For a review of IMS techniques see for example (and references therein): Clemmer, D. E.; Jarrold, M. F. Ion Mobility Measurements and Their Applications to Clusters and Biomolecules. *J. Mass Spectrom.* **1997,** *32,* 577–592.
3. For a review of IMS techniques see for example (and references therein): Hoaglund-Hyzer, C. S.; Counterman, A. E.; Clemmer, D. E. Anhydrous Protein Ions. *Chem. Rev.* **1999,** *99,* 3037–3079.
4. For a review of IMS techniques see for example (and references therein): Collins, D. C.; Lee, M. L. Developments in Ion Mobility Spectrometry-Mass Spectrometry. *Anal. Bioanal. Chem.* **2002,** 372, 66–73.
5. Revercomb, H. E.; Mason, E. A. Theory of Plasma Chromatography/Gaseous Electrophoresis. *Anal. Chem.* **1975,** *47,* 970–983.
6. Mason, E. A.; McDaniel, E. W. *Transport Properties of Ions in Gases*, Wiley, New York, 1988.
7. Liu, X.; Valentine, S. J.; Plasencia, M. D.; Trimpin, S.; Naylor, S.; Clemmer, D. E. Mapping the Human Plasma Proteome by SCX-LC-IMS-MS. *J. Am. Soc. Mass Spectrom.* **2007,** *18,* 1249–1264.
8. Valentine, S. J.; Plasencia, M. D.; Liu, X.; Krishnan, M.; Naylor, S.; Udseth, H. R.; Smith, R. D.; Clemmer, D. E. Toward Plasma Proteome Profiling with Ion Mobility-Mass Spectrometry. *J. Proteome Res.* **2006,** *5,* 2977–2984.
9. Valentine, S. J.; Counterman, A. E.; Hoaglund-Hyzer, C. S.; Clemmer, D. E. Gas-Phase Separations of Protease Digests. *J. Am. Soc. Mass Spectrom.* **1998,** *9,* 1213–1216.
10. Valentine, S. J.; Kulchania, M.; Barnes, C. A. S.; Clemmer, D. E. Multidimensional Separations of Complex Peptide Mixtures: A Combined High-Performance Liquid Chromatography/Ion Mobility/Time-of-Flight Mass Spectrometry Approach. *Int. J. Mass Spectrom.* **2001,** *212,* 97–109.
11. Matz, L. M.; Dion, H. M.; Hill, H. H. Evaluation of Capillary Liquid Chromatography-Electrospray Ionization Ion Mobility Spectrometry with Mass Spectrometry Detection. *J. Chromatogr. A* **2002,** *946,* 59–68.
12. Matz, L. M.; Asbury, G. R.; Hill, H. H. Two-Dimensional Separations with Electrospray Ionization Ambient Pressure High-Resolution Ion Mobility Spectrometry/Quadrupole Mass Spectrometry. *Rapid Commun. Mass Spectrom.* **2002,** *16,* 670–675.
13. Ruotolo, B. T.; Gillig, K. J.; Stone, E. G.; Russell, D. H. Peak Capacity of Ion Mobility Mass Spectrometry: Separation of Peptides in Helium Buffer Gas. *J. Chromatogr. B* **2002,** *782,* 385–392.
14. McLean, J. A.; Ruotolo, B. T.; Gillig, K. J.; Russell, D. H. Ion Mobility-Mass Spectrometry: A New Paradigm for Proteomics. *Int. J. Mass Spectrom.* **2005,** *240,* 301–315.
15. McLean, J. A.; Ridenour, W. B.; Caprioli, R. M. Profiling and Imaging of Tissues by Imaging Ion Mobility-Mass Spectrometry. *J. Mass Spectrom.* **2007,** *42,* 1099–1105.
16. Fenn, L. S.; McLean, J. A. Biomolecular Structural Separations by Ion Mobility-Mass Spectrometry. *Anal. Bioanal. Chem.* **2008,** *391,* 905–909.
17. Von Helden, G.; Hsu, M.-T.; Kemper, P. R.; Bowers, M. T. Structures of Carbon Cluster Ions from 3 to 60 Atoms: Linears to Rings to Fullerenes. *J. Chem. Phys.* **1991,** *95,* 3835–3837.
18. Jarrold, M. F.; Constant, V. A. Silicon Cluster Ions: Evidence for a Structural Transition. *Phys. Rev. Lett.* **1991,** *67,* 2994–2997.
19. Von Helden, G.; Hsu, M.-T.; Gotts, N.; Bowers, M. T. Carbon Cluster Cations with up to 84 Atoms: Structures, Formation Mechanism, and Reactivity. *J. Phys. Chem.* **1993,** *97,* 8182–8192.
20. Shelimov, K. B.; Hunter, J. M.; Jarrold, M. F. Small Carbon Rings: Dissociation, Isomerization, and a Simple Model Based on Strain. *Int. J. Mass Spectrom. Ion. Phys.* **1994,** *138,* 17–31.
21. Clemmer, D. E.; Hudgins, R. R.; Jarrold, M. F. Naked Protein Conformations: Cytochrome c in the Gas Phase. *J. Am. Chem. Soc.* **1995,** *117,* 10141–10142.
22. Mesleh, M. F.; Hunter, J. M.; Shvartsburg, A. A.; Schatz, G. C.; Jarrold, M. F. Structural Information from Ion Mobility Measurements: Effects of the Long-Range Potential. *J. Phys. Chem.* **1996,** *100,* 16082–16086.
23. Shvartsburg, A. A.; Jarrold, M. F. An Exact Hard-Spheres Scattering Model for the Mobilities of Polyatomic Ions. *Chem. Phys. Lett.* **1996,** *261,* 86–91.

24. Wyttenbach, T.; Von Helden, G.; Batka, J. J., Jr.; Carlat, D.; Bowers, M. T. Effect of the Long-Range Potential on Ion Mobility Measurements. *J. Am. Soc. Mass Spectrom.* **1997,** *8,* 275–282.
25. Valentine, S. J.; Anderson, J. G.; Ellington, A. D.; Clemmer, D. E. Disulfide-Intact and -Reduced Lysozyme in the Gas Phase: Conformations and Pathways of Folding and Unfolding. *J. Phys. Chem. B* **1997,** *101,* 3891–3900.
26. Hudgins, R. R.; Ratner, M. A.; Jarrold, M. F. Design of Helices That Are Stable In Vacuo. *J. Am. Chem. Soc.* **1998,** *120,* 12974–12975.
27. Counterman, A. E.; Clemmer, D. E. Large Anhydrous Polyalanine Ions: Evidence for Extended Helices and Onset of a More Compact State. *J. Am. Chem. Soc.* **2001,** *123,* 1490–1498.
28. Myung, S.; Badman, E.; Lee, Y. J.; Clemmer, D. E. Structural Transitions of Electrosprayed Ubiquitin Ions Stored in an Ion Trap over ~ 10 ms to 30 s. *J. Phys. Chem. A* **2002,** *106,* 9976–9982.
29. Rosell-Llompart, J.; Loscertales, I. G.; Bingham, D.; de la Mora, J. F. Sizing Nanoparticles and Ions with a Short Differential Mobility Analyzer. *J. Aerosol. Sci.* **1996,** *27,* 695–719.
30. Labowsky, M.; de la Mora, J. F. Novel Ion Mobility Analyzers and Filters. *J. Aerosol. Sci.* **2006,** *37,* 340–362.
31. McMurry, P. H. A Review of Atmospheric Aerosol Measurements. *Atmos. Environ.* **2000,** *34,* 1959–1999.
32. Purves, R. W.; Guevremont, R.; Day, S.; Pipich, C. W.; Matyjaszcayk, M. S. Mass Spectrometric Characterization of a High-Field Asymmetric Waveform Ion Mobility Spectrometer. *Rev. Sci. Instrum.* **1998,** *69,* 4094–4105.
33. Purves, R. W.; Guevremont, R. Electrospray Ionization High-Field Asymmetric Waveform Ion Mobility Spectrometry-Mass Spectrometry. *Anal. Chem.* **1999,** *71,* 2346–2357.
34. Eiceman, G. A.; Tadjikov, B.; Krylov, E.; Nazarov, E. G.; Miller, R. A.; Westbrook, J.; Funk, P. Miniature Radio-Frequency Mobility Analyzer as a Gas Chromatographic Detector for Oxygen-Containing Volatile Organic Compounds, Pheromones and Other Insect Attractants. *J. Chromatogr. A* **2001,** *917,* 205–217.
35. Shvartsburg, A. A.; Tang, K.; Smith, R. D. Modeling the Resolution and Sensitivity of FAIMS Analyses. *J. Am. Soc. Mass Spectrom.* **2004,** *15,* 1487–1498.
36. Venne, K.; Bonneil, E.; Eng, K.; Thibault, P. Improvement in Peptide Detection for Proteomics Analyses Using NanoLC-MS and High-Field Asymmetry Waveform Ion Mobility Mass Spectrometry. *Anal. Chem.* **2005,** *77,* 2176–2186.
37. Shvartsburg, A. A.; Li, F.; Tang, K.; Smith, R. D. High-Resolution Field Asymmetric Waveform Ion Mobility Spectrometry Using New Planar Geometry Analyzers. *Anal. Chem.* **2006,** *78,* 3706–3714.
38. Shvartsburg, A. A.; Mashkevich, S. V.; Smith, R. D. Feasibility of Higher-Order Differential Ion Mobility Separations Using New Asymmetric Waveforms. *J. Phys. Chem. A* **2006,** *110,* 2663–2673.
39. Henderson, S. C.; Valentine, S. J.; Counterman, A. E.; Clemmer, D. E. ESI/Ion Trap/Ion Mobility/Time-of-Flight Mass Spectrometry for Rapid and Sensitive Analysis of Biomolecular Mixtures. *Anal. Chem.* **1999,** *71,* 291–301.
40. Srebalus, C. A.; Li, J.; Marshall, W. S.; Clemmer, D. E. Gas-Phase Separations of Electrosprayed Peptide Libraries. *Anal. Chem.* **1999,** *71,* 3918–3927.
41. Asbury, G. R.; Klasmeier, J.; Hill, H. H., Jr. Analysis of Explosives Using Electrospray Ionization/Ion Mobility Spectrometry (ESI/IMS). *Talanta* **2000,** *50,* 1291–1298.
42. Asbury, G. R.; Wu, C.; Siems, W. F.; Hill, H. H. Separation and Identification of Some Chemical Warfare Degradation Products Using Electrospray High Resolution Ion Mobility Spectrometry with Mass Selected Detection. *Anal. Chim. Acta* **2000,** *404,* 273–283.
43. Steiner, W. E.; Clowers, B. H.; Haigh, P. E.; Hill, H. H. Secondary Ionization of Chemical Warfare Agent Simulants: Atmospheric Pressure Ion Mobility Time-of-Flight Mass Spectrometry. *Anal. Chem.* **2003,** *75,* 6068–6076.
44. Counterman, A. E.; Hilderbrand, A. E.; Srebalus Barnes, C. A.; Clemmer, D. E. Formation of Peptide Aggregates during ESI: Size, Charge, Composition, and Contributions to Noise. *J. Am. Soc. Mass Spectrom.* **2001,** *12,* 1020–1035.
45. Steiner, W. E.; Harden, C. S.; Hong, F.; Klopsch, S. J.; Hill, H. H.; McHugh, V. M. Detection of Aqueous Phase Chemical Warfare Agent Degradation Products by Negative Mode Ion Mobility Time-of-Flight Mass Spectrometry [IM(tof)MS]. *J. Am. Soc. Mass Spectrom.* **2006,** *17,* 241–245.
46. St. Louis, R. H.; Siems, W. F.; Hill, H. H., Jr. Ion Mobility Detection after Capillary Gas Chromatography. *LC-GC* **1988,** *6,* 810–814.
47. Chen, Y. H.; Hill, H. H., Jr.; Wittmer, D. P. Analytical Merit of Electrospray Ion Mobility Spectrometry as a Chromatographic Detector. *J. Microcolumn Sep.* **1994,** *6,* 515–524.
48. Chen, Y. H.; Siems, W. F.; Hill, H. H., Jr. Fourier Transform Electrospray Ion Mobility Spectrometry. *Anal. Chim. Acta* **1996,** *334,* 75–84.
49. Hoaglund, C. S.; Valentine, S. J.; Sporleder, C. R.; Reilly, J. P.; Clemmer, D. E. Three-Dimensional Ion Mobility/TOFMS Analysis of Electrosprayed Biomolecules. *Anal. Chem.* **1998,** *70,* 2236–2242.
50. Bluhm, B. K.; Gillig, K. J.; Russell, D. H. Development of a Fourier-Transform Ion Cyclotron Resonance Mass Spectrometer-Ion Mobility Spectrometer. *Rev. Sci. Instrum.* **2000,** *71,* 4078–4086.
51. Gillig, K. J.; Ruotolo, B.; Stone, E. G.; Russell, D. H.; Fuhrer, K.; Gonin, M.; Schultz, A. J. Coupling High-Pressure MALDI with Ion Mobility/Orthogonal Time-of-Flight Mass Spectrometry. *Anal. Chem.* **2000,** *72,* 3965–3971.
52. Hoaglund-Hyzer, C. S.; Clemmer, D. E. Ion Trap/Ion Mobility/Quadrupole/Time-of-Flight Mass Spectrometry for Peptide Mixture Analysis. *Anal. Chem.* **2001,** *73,* 177–184.
53. Tang, K.; Shvartsburg, A. A.; Lee, H.-N.; Prior, D. C.; Buschbach, M. A.; Li, F.; Tolmachev, A. V.; Anderson, G. A.; Smith, R. D. High-Sensitivity Ion Mobility Spectrometry/Mass Spectrometry Using Electrodynamic Ion Funnel Interfaces. *Anal. Chem.* **2005,** *77,* 3330–3339.
54. Clowers, B. H.; Siems, W. F.; Hill, H. H.; Massick, S. M. Hadamard Transform Ion Mobility Spectrometry. *Anal. Chem.* **2006,** *78,* 44–51.
55. Mack, E. Average Cross-Sectional Areas of Molecules by Gaseous Diffusion Methods. *J. Am. Chem. Soc.* **1925,** *47,* 2468–2482.
56. Shvartsburg, A. A.; Hudgins, R. R.; Dugourd, P.; Jarrold, M. F. Structural Information from Ion Mobility Measurements: Applications to Semiconductor Clusters. *Chem. Soc. Rev.* **2001,** *30,* 26–35.
57. Hoaglund-Hyzer, C. S.; Lee, Y. J.; Counterman, A. E.; Clemmer, D. E. Coupling Ion Mobility Separations, Collisional Activation Techniques, and Multiple Stages of MS for Analysis of Complex Peptide Mixtures. *Anal. Chem.* **2002,** *74,* 992–1006.
58. Valentine, S. J.; Koeniger, S. L.; Clemmer, D. E. A Split-Field Drift Tube for Separation and Efficient Fragmentation of Biomolecular Ions. *Anal. Chem.* **2003,** *75,* 6202–6208.
59. Koeniger, S. L.; Valentine, S. J.; Myung, S.; Plasencia, M.; Lee, Y. J.; Clemmer, D. E. Development of Field Modulation in a Split-Field Drift Tube for High-Throughput Multidimensional Separations. *J. Proteome Res.* **2005,** *4,* 25–35.
60. Koeniger, S. L.; Merenbloom, S. I.; Valentine, S. J.; Jarrold, M. F.; Udseth, H. R.; Smith, R. D.; Clemmer, D. E. An IMS-IMS Analogue of MS-MS. *Anal. Chem.* **2006,** *78,* 4161–4174.
61. Clowers, B. H.; Dwivedi, P.; Steiner, W. E.; Hill, H. H.; Bendiak, B. Separation of Sodiated Isobaric Disaccharides and Trisaccharides Using Electrospray Ionization-Atmospheric Pressure Ion Mobility-Time of Flight Mass Spectrometry. *J. Am. Soc. Mass Spectrom.* **2005,** *16,* 660–669.